

# The Information Content of Voltage-Dependent Conductance Histograms

Gaibo Zhang,<sup>†,‡</sup> Mark A. Ratner,<sup>¶</sup> and Matthew G. Reuter<sup>\*,‡,§,¶</sup>

*Oak Ridge High School, Oak Ridge, Tennessee 37830, United States, Computer Science and  
Mathematics Division, Oak Ridge National Laboratory, Oak Ridge, Tennessee 37831,  
United States, Department of Chemistry, Northwestern University, Evanston, Illinois  
60208, United States, and Center for Nanophase Materials Sciences, Oak Ridge National  
Laboratory, Oak Ridge, Tennessee 37831, United States*

E-mail: mgreuter@u.northwestern.edu

---

\*To whom correspondence should be addressed

<sup>†</sup>Oak Ridge High School, Oak Ridge, Tennessee 37830, United States

<sup>‡</sup>Computer Science and Mathematics Division, Oak Ridge National Laboratory, Oak Ridge, Tennessee 37831, United States

<sup>¶</sup>Department of Chemistry, Northwestern University, Evanston, Illinois 60208, United States

<sup>§</sup>Center for Nanophase Materials Sciences, Oak Ridge National Laboratory, Oak Ridge, Tennessee 37831, United States

## Abstract

We investigate the information content of voltage-dependent conductance histograms, which have recently been used to experimentally assess the current-voltage response properties of electrode-molecule-electrode junctions. To this end, we first develop a theoretical framework for simulating conductance histograms and then employ several model systems to explore the effects of various physical quantities. Our simulations show that the skewness of the histogram peak reflects asymmetry in the molecule-electrode couplings and that bias-asymmetric shapes are only obtained when the molecule drops bias. Furthermore, these histograms readily establish that the current-voltage properties of electrode-molecule-electrode junctions are non-Ohmic, and we demonstrate the qualitative similarity of the static and differential conductance. Ultimately, this work provides tools and guidelines for extracting additional physical insight from existing experimental data.

**Keywords:** Electron Transport, Voltage-Dependent Conductance Histograms, Statistical Models

17 1 Introduction

18 Understanding how molecules conduct electric current when connected to electrodes is inter-  
 19 esting for both fundamental and applied reasons.<sup>1-4</sup> For instance, electron dynamics change  
 20 when the system is driven away from equilibrium, and the ability to control electric current  
 21 on molecular time- and length-scales may lead to improved photovoltaics, thermoelectrics,  
 22 and sensors. However, tools from conventional electronics are not readily applicable to single  
 23 molecules, which have an inherently quantum mechanical nature; unlike traditional systems,  
 24 molecules have a discrete number of conduction channels through which electric current can  
 25 flow.<sup>5,6</sup> Each channel has a conductance  $G$  between 0 and  $G_0 \equiv 2e^2/h$ , and, in this sense,  
 26 molecules exhibit quantized conductance.

27 Both theoretical and experimental investigations have explored the ramifications of quan-  
28 tized conductance over the last twenty years. Let us consider several examples. First,  
29 the number of active conduction channels through the system is key. In many cases, each  
30 molecule contributes a single channel (usually corresponding to the highest occupied or lowest  
31 unoccupied molecular orbital), but some molecules (including those with nearly degenerate  
32 energy levels) may yield multiple active channels.<sup>7–9</sup> Although theoretical techniques for es-  
33 timating the number of active channels have been developed,<sup>6</sup> such an analysis is usually  
34 left to intuition. Second, the molecule-electrode interfaces are critically important,<sup>10–26</sup> as  
35 often evidenced through the use of various chemical linker groups. It is also possible that  
36 one molecule can bind to the electrodes in several ways, each of which results in a different  
37 conductance.<sup>12,15,18,21,22,27–30</sup> Third, current-voltage profiles are usually non-Ohmic; that is,  
38 the conductance (alternatively, the resistance) changes with the applied bias  $V$ .<sup>2,31–33</sup> In this  
39 case, there are two inequivalent definitions for conductance, static  $G_s = I/V$  and differential  
40  $G_d = \partial I / \partial V$ , where  $I$  is the current.

41 Experimental efforts to measure molecular conductance are further complicated by ir-  
42 reproducibility.<sup>11–14,17,18,28,30,32–46</sup> It is generally difficult to controllably prepare electrode-  
43 molecule-electrode junctions; consequently, there is considerable variation from one experi-  
44 mental measurement to the next. To compound the issue, common experimental techniques,  
45 such as scanning tunneling microscope-based break junctions, cannot generally *determine*  
46 the microscopic geometric details of the system being measured.<sup>11,14,18,38–41,44,45</sup> As a result,  
47 the molecular conductance is statistically assessed from many (typically thousands or more)  
48 measurements through a histogram analysis.<sup>11,13,14,33–36,39,40,47</sup> In short, each histogram bin  
49 tallies the number of times a conductance in its range was measured.

50 Most experiments have employed conductance histograms to examine molecular conduc-  
51 tance at a fixed and small applied bias, perhaps 0.1 V. The resulting one-dimensional his-  
52 tograms (counts vs. conductance) are interpreted in several ways. First, the mode of the first  
53 histogram peak (*i.e.*, the most frequently measured conductance) is taken as the “average”

54 molecular conductance.<sup>11,14,17,32,34,35,44,47,48</sup> Second, the width of the peak is related to the  
55 adsorption chemistry of the molecule with the electrodes, which is a convolution of numerous  
56 factors, including temperature.<sup>13,16,17,32,36,37,44,48–51</sup> Finally, recent analyses have considered  
57 the peak’s line shape by applying probability theory<sup>52</sup> to electron transport problems.<sup>51,53</sup>  
58 These works reveal that the average level alignment of the molecule (i.e., the energy offset  
59 between the channel level and the Fermi level) and/or the average coupling strength between  
60 the channel and the electrodes are encoded in the conductance histogram peaks.<sup>30,46,51</sup>

61 Other studies have gone beyond these one-dimensional histograms and constructed vari-  
62 ous types of two-dimensional conductance histograms that further elucidate electron trans-  
63 port processes.<sup>20,30,43,45,54–56</sup> For the example of interest here, voltage-dependent histograms  
64 have recently been reported,<sup>43</sup> where a voltage scan is performed on each synthesized electrode-  
65 molecule-electrode junction. The resulting histogram has conductance and applied bias on  
66 the axes with a color map depicting the number of counts in each bin. Example experimental  
67 voltage-dependent histograms for static conductance are shown in Figure 1. In many cases,  
68 the voltage-dependent conductance histogram is bowl shaped and fairly symmetric about its  
69 minimum [Figure 1(a)]; however, other shapes are also observed [Figure 1(b)]. The chemistry  
70 underlying these histogram shapes is not well understood, and it has been hypothesized<sup>43</sup>  
71 that the asymmetric bowl (*i.e.*, not symmetric about its minimum) in Figure 1(b) is caused  
72 by asymmetric molecule-electrode couplings. Such asymmetric couplings may be the result  
73 of asymmetric molecular structure, the use of different linking groups, and/or differences in  
74 the two electrodes.

75 In this work we extend previous analyses of the line shapes of one-dimensional con-  
76 ductance histograms<sup>51,53</sup> to voltage-dependent conductance histograms. First, we develop  
77 a computational framework for simulating voltage-dependent conductance histograms that  
78 incorporates various physically-inspired model systems. We subsequently use simulated his-  
79 tograms to investigate the information content of voltage-dependent conductance histograms,  
80 with special interest in the experimental histograms of Figure 1 and Ref. 43. By comparing

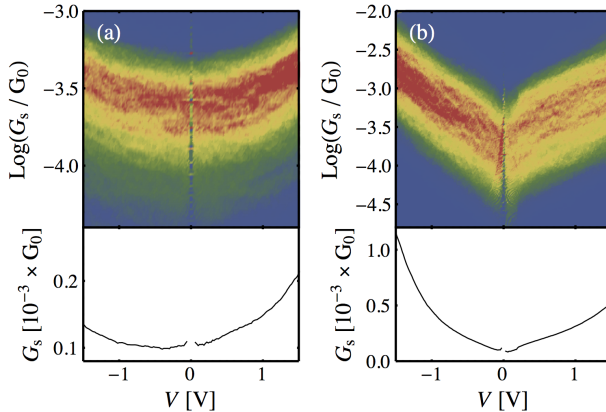


Figure 1: Experimental voltage-dependent histograms of static conductance for transport through (a) octanedithiol and (b) biphenyldithiol molecules. The color scales are arbitrary; red means many counts and blue means few. The bottom panels show the average conductance-voltage profiles of the upper panels, as determined from the statistical data in each histogram. In many cases,<sup>43</sup> bowl shapes that are symmetric about their minimum [panel (a)] are observed; however, asymmetric shapes [panel (b)] are also seen. This experimental data is from Ref. 43, and is used with permission.

81 results from the different model systems, we show that histograms with symmetric bowl  
 82 shapes [e.g., Figure 1(a)] are fairly common and that the location of the bowl's minimum  
 83 relates to the voltage drop across the junction. Asymmetric bowl shapes (around the bowl's  
 84 minimum), as in Figure 1(b), reflect more complicated chemistry. We find that asymmetric  
 85 molecule-electrode couplings do not cause the asymmetric bowl shape, and instead propose  
 86 that multiple active conduction channels are responsible for such a phenomenon. In essence,  
 87 each channel contributes a symmetric bowl shape and the sum of even two bowls can be  
 88 asymmetric about its minimum. In the course of this analysis, we discuss how to interpret  
 89 voltage-dependent histograms, explore the signatures of various effects in the histograms,  
 90 and compare the static and differential conductance through molecular systems.

91 The layout of this paper is as follows. We begin by developing our theory of conductance  
 92 histograms in Section 2. This section also describes the histogram simulator and details the  
 93 various model systems used throughout. Section 3 presents voltage-dependent conductance  
 94 histograms from the different models, exploring the signatures of (i) asymmetric molecule-  
 95 electrode coupling, (ii) bias-dependent physical parameters, and (iii) some multi-channel

96 effects. From this presentation we are able to establish the information content of voltage-  
97 dependent conductance histograms and offer guidelines on how to extract this data. Finally,  
98 we summarize the results and conclude in Section 4.

## 99 2 Simulating Conductance Histograms

100 In this section we discuss pertinent aspects of electron transport theory (Section 2.1), intro-  
101 duce the various model systems used to simulate voltage-dependent conductance histograms  
102 (Section 2.2), and finally describe our framework for simulating conductance histograms  
103 (Section 2.3).

### 104 2.1 Landauer-Büttiker Theory

105 Electron transport theories typically employ scattering theory to describe electron dynam-  
106 ics.<sup>2</sup> When we limit our attention to elastic, coherent scattering under steady-state condi-  
107 tions, we obtain the Landauer-Büttiker formalism,<sup>5,57</sup> which is often used to describe electric  
108 current through molecules. Conduction channels are central to this formalism, and each chan-  
109 nel has a probability of shuttling an electron with energy  $E$  between the electrodes. The sum  
110 of such transmission probabilities over all channels yields the transmission function,  $T(E)$ ,  
111 to which each channel usually contributes a Lorentzian-shaped component.

112 All of the transport quantities we seek to understand build upon the transmission func-  
113 tion. Consider the electric current,<sup>2</sup>

$$I(V) = \frac{2e}{h} \int_{-\infty}^{\infty} dE T(E; V) [f_L(E; V) - f_R(E; V)],$$

114 where  $f_L$  ( $f_R$ ) is the Fermi function of the left (right) electrode. Note that the Fermi functions  
115 and the transmission function generally depend on the applied bias. Because tunneling  
116 behavior is reasonably insensitive to temperature, it is convenient to work in the limit of

<sup>117</sup> zero temperature, where the Fermi functions become step functions. Then,

$$I(V) = \frac{2e}{h} \int_{E_F - eV/2}^{E_F + eV/2} dE T(E; V), \quad (1)$$

where  $E_F$  is the Fermi energy of the electrode-molecule-electrode junction. Finally, we can obtain expressions for both the static and differential conductance using Eq. (1). From their definitions,

$$\begin{aligned} G_s(V) &= \frac{I(V)}{V} \\ &= \frac{2e}{hV} \int_{E_F - eV/2}^{E_F + eV/2} dE T(E; V) \end{aligned} \quad (2)$$

is the static conductance and

$$\begin{aligned} G_d(V) &= \frac{\partial}{\partial V} I(V) \\ &= \frac{2e^2}{h} \frac{1}{2} [T(E_F + eV/2; V) + T(E_F - eV/2; V)] \\ &\quad + \frac{2e}{h} \int_{E_F - eV/2}^{E_F + eV/2} dE \frac{\partial}{\partial V} T(E; V) \end{aligned} \quad (3)$$

<sup>118</sup> is the differential conductance.

## <sup>119</sup> 2.2 Model Systems

<sup>120</sup> The Landauer-Büttiker formalism introduced in the previous subsection shows how to calculate  
<sup>121</sup> the static or differential conductance through an electrode-molecule-electrode junction,  
<sup>122</sup> up to obtaining the transmission function. We now detail, in this subsection, the three models  
<sup>123</sup> we use to generate transmission functions and subsequently investigate voltage-dependent  
<sup>124</sup> conductance histograms.

Before introducing the models, let us first discuss the necessary elements of a model junction and how they determine  $T(E)$ . There are three key components: (i) the Hamiltonian of the isolated molecule (channel),  $\mathbf{H}$ ; (ii) a self-energy,  $\Sigma_L(E)$ , describing how the isolated molecule couples to the left electrode; and (iii) a similar self-energy,  $\Sigma_R(E)$ , for the right electrode. Note that the self-energies are non-Hermitian operators that essentially encapsulate open-system boundary conditions. From these,<sup>2</sup>

$$T(E) = \text{Tr} [\mathbf{G}(E)\boldsymbol{\Gamma}_L(E)\mathbf{G}^\dagger(E)\boldsymbol{\Gamma}_R(E)], \quad (4a)$$

where

$$\mathbf{G}(E) = [E\mathbf{I} - \mathbf{H} - \Sigma_L(E) - \Sigma_R(E)]^{-1} \quad (4b)$$

is the Green function,<sup>58</sup>  $\mathbf{I}$  is the identity operator, and

$$\boldsymbol{\Gamma}_{L/R}(E) = i \left[ \Sigma_{L/R}(E) - \Sigma_{L/R}^\dagger(E) \right] \quad (4c)$$

is the spectral density for coupling to the left/right electrode. We write all of these operators as matrices in the following discussion, where, for simplicity, we assume an orthonormal basis set.

The simplest model junction consists of a single channel that couples symmetrically to both electrodes. The model parameters will generally depend on the bias, reflecting the fact that bias drops through the molecule. For simplicity, we only consider voltage-dependent level energies; voltage-dependent couplings produce similar results. Mathematically,  $\mathbf{H} = [\varepsilon + aeV]$  and  $\Sigma_L(E) = \Sigma_R(E) = [-i\Gamma/2]$ , where  $\varepsilon$  is the channel's energy level,  $a$  is a scaling factor, and  $\Gamma > 0$  is the effective channel-electrode coupling. Using Eq. (4),

$$T(E) = \frac{\Gamma^2}{(E - \varepsilon - aeV)^2 + \Gamma^2} \quad (5a)$$

<sup>142</sup> is Lorentzian, as expected. Then, from Eqs. (2) and (3),

$$G_s(V) = \frac{2e\Gamma}{hV} \left[ \arctan \left( \frac{E_F - \varepsilon + (1/2 - a)eV}{\Gamma} \right) - \arctan \left( \frac{E_F - \varepsilon - (1/2 + a)eV}{\Gamma} \right) \right] \quad (5b)$$

<sup>143</sup> and

$$G_d(V) = \frac{2e^2}{h} \left[ \frac{(1/2 - a)\Gamma^2}{[E_F - \varepsilon + (1/2 - a)eV]^2 + \Gamma^2} + \frac{(1/2 + a)\Gamma^2}{[E_F - \varepsilon - (1/2 + a)eV]^2 + \Gamma^2} \right], \quad (5c)$$

<sup>144</sup> respectively.

<sup>145</sup> Our second model is very similar to the first, but now allows asymmetric coupling to the  
<sup>146</sup> electrodes. As before,  $\mathbf{H} = [\varepsilon + aeV]$ ; however,  $\Sigma_L(E) = [-i\Gamma_L/2]$  and  $\Sigma_R(E) = [-i\Gamma_R/2]$   
<sup>147</sup> for coupling elements  $\Gamma_L > 0$  and  $\Gamma_R > 0$ . Then,

$$T(E) = \frac{4\Gamma_L\Gamma_R}{4(E - \varepsilon - aeV)^2 + (\Gamma_L + \Gamma_R)^2}, \quad (6a)$$

$$G_s(V) = \frac{4e\Gamma_L\Gamma_R}{hV(\Gamma_L + \Gamma_R)} \left[ \arctan \left( \frac{2[E_F - \varepsilon + (1/2 - a)eV]}{\Gamma_L + \Gamma_R} \right) - \arctan \left( \frac{2[E_F - \varepsilon - (1/2 + a)eV]}{\Gamma_L + \Gamma_R} \right) \right], \quad (6b)$$

and

$$G_d(V) = \frac{2e^2}{h} \left[ \frac{4(1/2 - a)\Gamma_L\Gamma_R}{4[E_F - \varepsilon + (1/2 - a)eV]^2 + (\Gamma_L + \Gamma_R)^2} + \frac{4(1/2 + a)\Gamma_L\Gamma_R}{4[E_F - \varepsilon - (1/2 + a)eV]^2 + (\Gamma_L + \Gamma_R)^2} \right]. \quad (6c)$$

<sup>148</sup>

<sup>149</sup> The final model examines multi-channel effects by combining two independent conduction  
<sup>150</sup> channels that are each described by the first model [Eqs. (5a)–(5c)]. Mathematically,  $\mathbf{H} =$   
<sup>151</sup>  $\text{diag}(\varepsilon_1 + a_1 eV, \varepsilon_2 + a_2 eV)$  and  $\Sigma_{L/R}(E) = \text{diag}(-i\Gamma_1/2, -i\Gamma_2/2)$ , where the subscripts are

152 a channel index. Although this model might initially appear somewhat *ad hoc*, any two  
153 channel system can be written as the sum of two independent channels using, for instance,  
154 an eigenchannel decomposition.<sup>6</sup> The static (differential) conductance through the entire  
155 system is simply the sum of both channels' static (differential) conductances.

### 156 2.3 Conductance Histograms as Probability Density Functions

157 Our theory for conductance histograms begins with the idea that the various model pa-  
158 rameters (e.g.,  $\varepsilon$ ,  $\Gamma_L$ , etc.) behind electron transport are random variables.<sup>48,51,53</sup> Figure  
159 2 depicts this concept for a generic model system. In essence, we equate the experimen-  
160 tal irreproducibility when measuring conductance with stochasticity; each parameter has  
161 an underlying probability distribution and every measurement samples from these distribu-  
162 tions. The conductance histogram therefore reports the probability density function<sup>52</sup> for  
163 the conductance observable, which is directly determined by the distributions of the model  
164 parameters.<sup>51</sup>

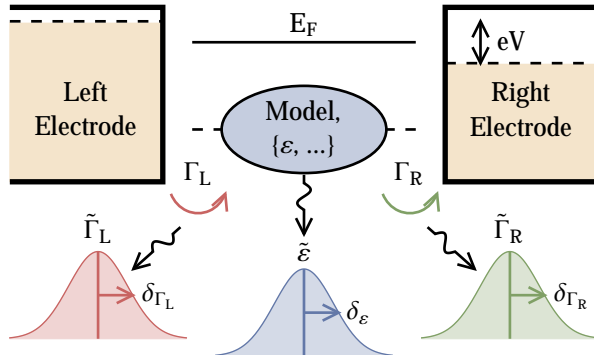


Figure 2: Schematic of our framework for simulating voltage-dependent conductance his-  
 tograms. A model system (Section 2.2) is placed between two electrodes and a bias ( $V$ ) is  
 applied across the junction. The model system (blue) depends on several physical quantities  
 such as the channel energy ( $\varepsilon$ ). The conduction channel(s) in the model system couple to the  
 left (right) electrode with  $\Gamma_L$  ( $\Gamma_R$ ), and the Fermi energies of the two electrodes (dashed lines)  
 are offset from the junction Fermi energy ( $E_F$ ) by the bias. When constructing histograms,  
 we assume that each of these physical parameters is an independent random variable. As  
 depicted by the normal distributions, each conductance “measurement” samples from the  
 probability distributions of these parameters.

165 This realization facilitates the simulation of conductance histograms. Simply put, we  
166 emulate each conductance measurement by using a random number generator to sample from  
167 the model parameters' distributions (and then compute conductance as described in Section  
168 2.2). Unless otherwise specified, we use normal distributions for each parameter; notationally,  
169  $\tilde{\varepsilon}$  and  $\delta_\varepsilon$  denote the average and standard deviation for  $\varepsilon$ , respectively, and likewise for  
170 other parameters. Mimicking experiment, we then compile many simulated conductance  
171 values into a histogram. By changing the distributions of the parameters or the underlying  
172 model, the signatures of specific physical properties in a conductance histogram can be  
173 investigated. We implemented this simulation framework for many model systems in C++11  
174 using the random number generation tools in the GNU Scientific Library (GSL).<sup>59</sup> Our  
175 software, MolStat, is available open source<sup>60</sup> and can readily generate any of the histograms  
176 reported herein. Specific MolStat input files are presented in the Supporting Information.

### 177 3 Results & Discussion

178 Equipped with a framework for simulating voltage-dependent conductance histograms, we  
179 now turn to investigating the information content of the histograms. To develop intuition, we  
180 first consider a single channel that symmetrically couples to both electrodes and then grad-  
181 ually increase the model complexity to explore the signatures of, e.g., asymmetric channel-  
182 electrode coupling and multi-channel effects.

#### 183 3.1 One Channel with Symmetric Electrode Coupling

184 As discussed in Section 2.2, the simplest model for conductance through an electrode-  
185 molecule-electrode junction is a single channel that couples symmetrically to both elec-  
186 trodes. Accordingly, Figure 3(a) shows the characteristic Lorentzian transmission function  
187 for transport through such a channel. The Lorentzian peaks at one, indicating a resonant  
188 energy where the junction always transmits the electron, and asymptotically decays for

energies away from the resonance. Although resonant tunneling is common for transport through some systems (e.g., point contacts),<sup>51</sup> transport through molecules is typically far from resonance. We focus on this non-resonant tunneling regime in what follows such that the molecular junction's Fermi energy  $E_F$  falls in one of the Lorentzian's tails.

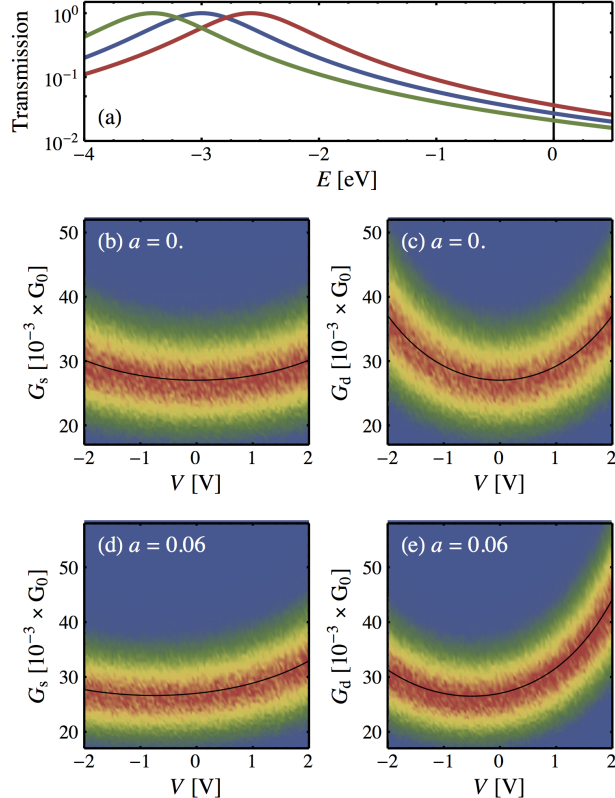


Figure 3: Example voltage-dependent conductance histograms for a single channel that couples symmetrically to both electrodes. (a) Transmission spectrum of the channel for the average model parameters  $\tilde{\varepsilon} = -3$  eV and  $\tilde{\Gamma} = 0.5$  eV. The blue line shows the case where  $V = 0$  V or  $a = 0$ ; for  $a > 0$ , negative biases shift the resonance to more negative energies (green line) and positive biases shift it to more positive energies (red line). The vertical line shows the Fermi energy ( $E_F = 0$  eV) used for generating the histograms. (b)–(e): Simulated conductance histograms with  $\delta_\varepsilon = \delta_\Gamma = 0.05$  eV and the indicated  $a$ . Red (blue) indicates a large (small) probability of observing the conductance ( $G_s$  or  $G_d$  at the bias  $V$ ); the absolute scale is arbitrary. The left and right columns show the static and differential conductances, respectively. In all cases, the conductance for the average physical parameters ( $\tilde{\varepsilon}$  and  $\tilde{\Gamma}$ , shown as a black line) traces out the histogram shape. These histograms display the characteristic symmetric bowl shape [see Figure 1(a)];<sup>43</sup> the voltage drop across the molecule ( $a$ ) determines the location of the bowl's minimum.

This Lorentzian-tail shape near  $T(E_F)$  gives one-dimensional histograms a characteristic

<sup>194</sup> line shape for non-resonant tunneling.<sup>51,53</sup> We now seek to determine how the Lorentzian-  
<sup>195</sup> tail is manifested in voltage-dependent conductance histograms. Following the procedure in  
<sup>196</sup> Section 2.3, we assume  $\varepsilon$  and  $\Gamma$  are random variables with normal distributions and proceed  
<sup>197</sup> to simulate one million conductance “measurements” for each histogram. The average values  
<sup>198</sup>  $\tilde{\varepsilon}$  and  $\tilde{\Gamma}$  are taken to be the  $\varepsilon$  and  $\Gamma$  used in the transmission function of Figure 3(a), and the  
<sup>199</sup> Fermi energy is detuned from resonance [black line in Figure 3(a)]. Note that the specific  
<sup>200</sup> values of  $\tilde{\varepsilon} (\pm \delta_\varepsilon)$ ,  $\tilde{\Gamma} (\pm \delta_\Gamma)$ , and  $E_F$  do not qualitatively affect our analysis so long as  $E_F$  is  
<sup>201</sup> sufficiently far from resonance to fall in either tail of the Lorentzian.

<sup>202</sup> Let us first consider the case where voltage does not drop across the molecule,  $a = 0$ .  
<sup>203</sup> For such a system, Figures 3(b) and 3(c) display simulated voltage-dependent histograms  
<sup>204</sup> of the static and differential conductance, respectively. There are four noteworthy obser-  
<sup>205</sup> vations. First, and most strikingly, these histograms have the symmetric bowl shape seen  
<sup>206</sup> experimentally [Figure 1(a)], although each simulated bowl’s minimum always occurs at  
<sup>207</sup>  $V = 0$  V. A careful inspection of Eq. (5) shows that  $G_{s/d}(V) = G_{s/d}(-V)$  when  $a = 0$ ;  
<sup>208</sup> the lack of a voltage drop through the molecule results in symmetry for positive and nega-  
<sup>209</sup> tive biases. Second, the histograms’ shapes match the “average” conductances obtained by  
<sup>210</sup> evaluating  $G_{s/d}(V)$  with the average parameters  $\tilde{\varepsilon}$  and  $\tilde{\Gamma}$ . These “averages” are displayed  
<sup>211</sup> as black lines superimposed on the histograms and also coincide with the expected conduc-  
<sup>212</sup> tances (the statistical averages) in both cases. Third, a close examination of the histograms  
<sup>213</sup> reveals that the average conductance (black line) is typically a bit larger than the mode  
<sup>214</sup> of the histogram (approximately the middle of the red band), indicating that the peak is  
<sup>215</sup> positively skewed. (Crudely, positive skewness means that the peak has a longer tail above  
<sup>216</sup> the mode than below.) This generalizes previous analyses of zero-bias conductance<sup>53</sup> in  
<sup>217</sup> relating positive skewness to transport via non-resonant tunneling. Lastly, the histograms  
<sup>218</sup> confirm that transport in molecular systems is non-Ohmic because the static and differential  
<sup>219</sup> conductances are both different and dependent on the bias. It is interesting to note that the  
<sup>220</sup> differential conductance is steeper than the static conductance, which is a consequence of

their definitions.  $G_s \equiv I/V$  has a “memory” of all smaller biases whereas  $G_d \equiv \partial I/\partial V$  does not; the differential conductance is more sensitive to the non-Ohmic behavior. Regardless, the static and differential conductance histograms are qualitatively very similar, a trend that holds in every case to follow. As a result, we only explicitly consider the static conductance histograms in the subsequent discussion.

We can now examine the effect of a voltage drop across the molecule ( $a \neq 0$ ) on voltage-dependent conductance histograms. To begin, Figure 3(a) shows the transmission function (evaluated with the average parameters) for several biases and  $a > 0$  ( $a < 0$  creates opposite effects). As expected, the resonance energy now depends on  $V$ , breaking the symmetry between positive and negative biases. In the pictured case, positive biases bring the resonance closer to  $E_F$ , whereas negative biases shift it away.

Turning to the histograms, Figures 3(d) and 3(e) display simulated histograms for the same parameters as above, except  $a = 0.06$ . Similar to before, these histograms exhibit the symmetric bowl shape (the arms are roughly the same on both sides of the minimum); however, each bowl’s minimum is now shifted off of  $V = 0$  V. Furthermore, Figure 3(d) qualitatively matches the experimental histogram in Figure 1(a). It seems that this symmetric bowl shape reflects transport through a fairly simple system, and the location of the bowl’s minimum provides information on the amount of voltage dropped across the molecule.

Finally, we note that this model—a single channel with a bias-dependent channel energy—does not reproduce the histogram shape seen in Figure 1(b). Even though  $a$  moves the voltage of bowl’s minimum, the arms of the bowl remain mostly symmetric. It is conceivable, however, that  $\Gamma$  may depend on the bias (instead of, or in addition to,  $\varepsilon$ ). If we suppose that  $\Gamma \rightarrow \Gamma + beV$  (for some  $b$ ) and that  $\varepsilon$  is independent of  $V$ , we can again derive static and differential conductances with Eqs. (2) and (3). Although we omit the results, such a model also produces histograms with symmetric bowl shapes. It appears that single-channel models with symmetric electrode-channel couplings cannot reproduce the asymmetric bowl shape in Figure 1(b) without some complicated bias dependence on  $\varepsilon$  and/or  $\Gamma$ . Inferring

248 the bias dependence of these parameters from an experimental histogram, which amounts to  
249 solving an inverse problem, could be interesting, but we will continue to search for a more  
250 intuitive explanation.

## 251 3.2 One Channel with Asymmetric Electrode Coupling

252 It was hypothesized<sup>43</sup> that the asymmetric bowl shape (*i.e.*, the bowl is not symmetric about  
253 its minimum) in Figure 1(b) is caused by asymmetric couplings between the channel and  
254 the electrodes. This explanation is certainly plausible, and is easy to investigate with our  
255 histogram simulator. Throughout this discussion we use the ratio

$$\xi \equiv \frac{\max(\tilde{\Gamma}_L, \tilde{\Gamma}_R)}{\min(\tilde{\Gamma}_L, \tilde{\Gamma}_R)}$$

256 to quantify the degree of asymmetric coupling (in an average sense).

257 Switching to the model system with a single channel that couples asymmetrically to the  
258 electrodes (the second model in Section 2.2), we simulate voltage-dependent conductance  
259 histograms with varying degrees of asymmetric coupling. The model parameters are similar  
260 to those used in the previous section; specifically, the distribution for  $\varepsilon$  is unchanged,  $\Gamma_L$   
261 has the same distribution as  $\Gamma$ , and the distribution of  $\Gamma_R$  is chosen to yield the desired  
262  $\xi$ . As before, we note that our analysis does not qualitatively change if any of the model  
263 parameters are perturbed (assuming  $E_F$  still leads to non-resonant tunneling).

264 To isolate the effects of coupling asymmetry, we first take  $a = 0$ ; Figures 4(b) and  
265 4(c) show the case of  $\xi = 1$ , where the *average* channel is symmetrically coupled to both  
266 electrodes. Although most samples will be asymmetrically coupled,  $\Gamma_L$  and  $\Gamma_R$  should still be  
267 approximately equal. Even though there is slight asymmetry in the couplings, the primary  
268 observation in these histograms is that the bowl shape remains symmetric about its minimum  
269 (and also around  $V = 0$  V because  $a = 0$ ). Of secondary interest, the average conductance  
270 (black line) again matches each histogram's shape.

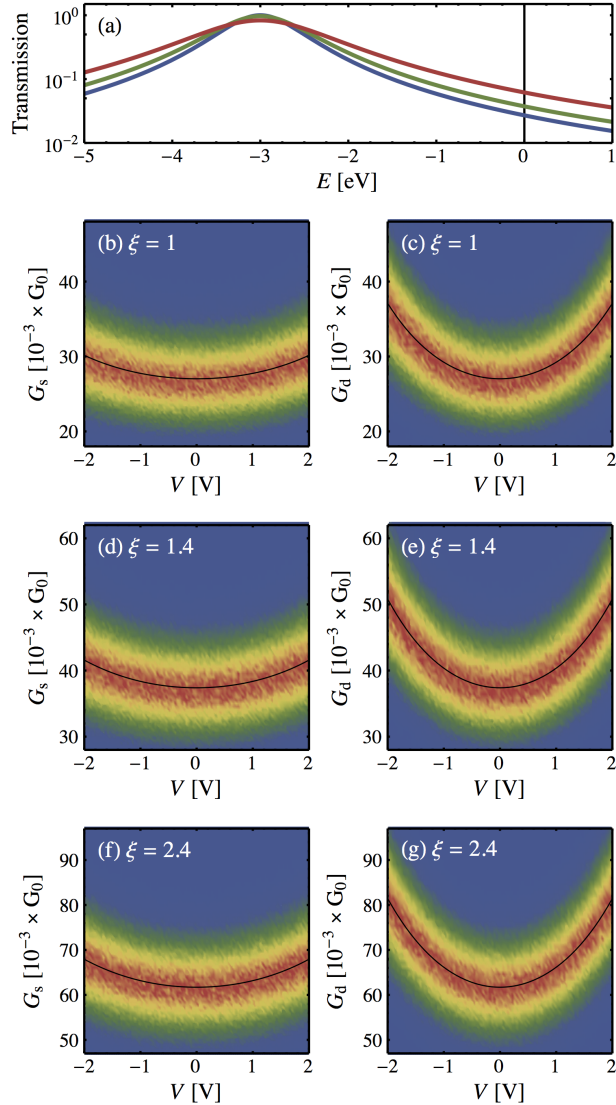


Figure 4: Example voltage-dependent conductance histograms for a single channel that does not drop voltage and that couples asymmetrically to the electrodes; the panels are similar to those in Figure 3. (a) Transmission functions for channels with average parameters:  $\tilde{\varepsilon} = -3$  eV  $\tilde{\Gamma}_L = 0.5$  eV, and  $a = 0$  for all cases,  $\tilde{\Gamma}_R = 0.5$  eV ( $\xi = 1$ ) for the blue curve,  $\tilde{\Gamma}_R = 0.7$  eV ( $\xi = 1.4$ ) for the green curve, and  $\tilde{\Gamma}_R = 1.2$  eV ( $\xi = 2.4$ ) for the red curve. The vertical line shows the Fermi level ( $E_F = 0$  eV) used for generating the histograms. (b)–(g) Simulated conductance histograms for  $\delta_\varepsilon = \delta_{\Gamma_L} = \delta_{\Gamma_R} = 0.05$  eV, and the indicated  $\xi$ . As in the symmetrically coupled model, the conductance for the average parameters closely traces the bowl-shaped histogram. In all cases, however, the bowls in the conductance histograms are symmetric about their minima; asymmetry in the electrode-channel couplings is not responsible for the asymmetric bowl shape in Figure 1(b).

We now increase the degree of asymmetry in the couplings to  $\xi = 1.4$  and show the resulting histograms in Figures 4(d) and 4(e). Asymmetric couplings are now more prevalent, but there is still a reasonable chance that  $\Gamma_L \approx \Gamma_R$  for some samples. As in the previous case, the histograms display the familiar bowl shape that is symmetric about its minimum. Finally, Figures 4(f) and 4(g) show histograms for  $\xi = 2.4$ , where it is very unlikely that  $\Gamma_L \approx \Gamma_R$ . The bowl shape in each histogram remains symmetric about its minimum.

All of the symmetric bowl-shaped histograms in Figure 4 consider a molecule that does not drop voltage ( $a = 0$ ). However, it is conceivable that the combination of asymmetric molecule-electrode couplings and a voltage drop across the molecule ( $a \neq 0$ ) may produce a bowl-shaped histogram that is asymmetric about its minimum. To investigate, Figure 5 displays simulated histograms using the same model parameters as in Figure 4 except that  $a = 0.06$ . Similar to Figures 3(d) and (e), the minimum of each bowl moves to non-zero biases when  $a \neq 0$ , but each bowl remains symmetric about its minimum. Furthermore, the qualitative shapes of the histograms in Figure 5 are not changed by increasing the asymmetry in the couplings.

It seems doubtful from these simulations that asymmetry in the molecule-electrode couplings is responsible for the asymmetric bowl shape in Figure 1(b). Even though each simulated bowl's minimum depends on the voltage dropped across the molecule, the two arms of the bowl are symmetric within this model. This observation reflects the arbitrariness of assigning the “left” and “right” labels to the electrodes.

Before exploring other potential causes for the asymmetric bowl shape in Figure 1(b), let us examine the signature of coupling asymmetry in the histograms by considering the skewness of one-dimensional slices from each histogram in Figure 4. A visual comparison of the average conductance (superimposed black line) to the mode of each histogram (middle of the red band) shows that the average conductance for a particular bias edges slightly closer to the mode as the degree of coupling asymmetry increases. It appears that skewness decreases as  $\xi$  increases.

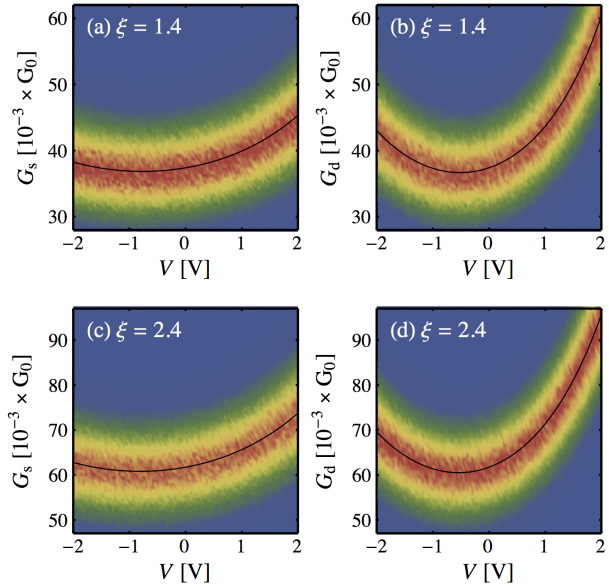


Figure 5: Example voltage-dependent conductance histograms for a single channel that drops voltage and couples asymmetrically to both electrodes. Except for  $a = 0.06$  here, panels (a)–(d) use the same parameters as panels (d)–(g) of Figure 4, respectively. As in the symmetrically coupled model, the minimum of the bowl shape is shifted to non-zero biases when voltage drops through the molecule. However, as in Figure 4, the bowls remain symmetric about their minima. Asymmetric coupling between the molecule and the electrodes does not cause a bowl shape that is asymmetric about its minimum.

298 We quantify this qualitative observation in Figure 6, where we show the skewness of  
 299 the histograms in Figure 4 as a function of the bias. (Each skewness reports the statistics  
 300 of a vertical slice from the voltage-dependent conductance histogram.) Although there is  
 301 some fluctuation in the skewness from one bias to another, it is apparent that the skewness  
 302 decreases, on average, as  $\xi$  increases. Thus, coupling asymmetry can be seen in the skewness  
 303 of the histogram peaks.

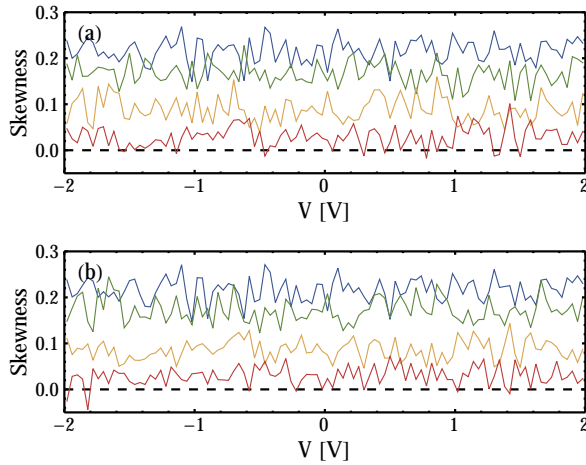


Figure 6: Skewness of the one-dimensional histogram peak as a function of the bias for the conductance histograms in Figure 4 (where a single channel couples asymmetrically to the electrodes). (a) Static conductance; (b) differential conductance. In both panels, blue is  $\xi = 1$ , green is  $\xi = 1.4$ , yellow is  $\xi = 2.4$ , and red is  $\xi = 4$ . As coupling asymmetry increases ( $\xi \rightarrow \infty$ ), the skewness of the histogram decreases (on average).

304 This relationship is explained by connecting the shape of the transmission function around  
 305  $E_F$  to the histogram's skewness.<sup>53</sup> The argument is as follows. The fluctuations inherent  
 306 to each conductance measurement cause us to sample different points on the transmission  
 307 function near  $E_F$ . For transport via non-resonant tunneling (where  $E_F$  is in the tails of  
 308 the Lorentzian),  $T(E)$  rises more quickly than it falls in this neighborhood. Consequently,  
 309 fluctuations are slightly more likely to increase the transmission, resulting in a positively-  
 310 skewed histogram peak.<sup>53</sup> Transmission functions with flatter tails will be more insulated  
 311 from this effect as larger fluctuations will be required to noticeably change the observed  
 312 transmission.

313 Returning to the relation between histogram skewness and coupling asymmetry, we ex-

314 amine the transmission functions for systems with various  $\xi$ . Figure 4(a) shows the average  
315 transmission function for each system with  $E_F$  marked by the vertical black line. When  
316  $\xi = 1$  [blue line in Figure 4(a)], the transmission function peaks at one and decays rapidly,  
317 as expected. Increasing  $\xi$  results in flatter transmission functions; that is, the peaks de-  
318 crease in magnitude and the tails decay less rapidly. Consequently, more asymmetry in the  
319 channel-electrode couplings leads to less skewed histogram peaks. Such asymmetric coupling  
320 does not, however, qualitatively change the shapes of voltage-dependent histograms.

### 321 3.3 Two Independent Channels

322 All of the results so far have explored model systems with a single channel. The symmetric  
323 bowl shape seen in Figure 1(a) is commonly observed, and we investigated the signatures  
324 of asymmetric electrode-channel couplings. None of these models, however, reproduce the  
325 asymmetric bowl shape for the biphenyldithiol junction in Figure 1(b). If we appeal to our  
326 chemical intuition, it may be that this molecule’s HOMO (highest occupied molecular orbital)  
327 and HOMO-1 (or LUMO and LUMO+1) produce nearly-degenerate conduction channels.  
328 Accordingly, let us examine some multi-channel effects in conductance histograms.

329 From Section 2.2, the simplest system for investigating multi-channel effects consists of  
330 two independent channels, which may result from an eigenchannel decomposition<sup>6</sup> of the  
331 system. We suppose that each channel drops bias (*i.e.*, it is described by the single-channel  
332 models), meaning that the histogram for either channel would produce a bowl shape that  
333 is symmetric around its minimum. As seen in Figures 3 and 5, the location of each bowl’s  
334 minimum depends on the voltage drop through the respective channel.

335 Consider now the histogram for both channels, which is the “sum” of the two channels’  
336 histograms. If  $a_1$  and  $a_2$  (the voltage drop parameters through the two channels) have the  
337 same sign, then the composite histogram will display a bowl shape with a minimum shifted  
338 further from  $V = 0$  V than either of the independent channels. This resulting bowl may also  
339 be asymmetric around its minimum. Examples are displayed in Figures 7(a) and (b). On

the other hand, if  $a_1$  and  $a_2$  have opposite signs, one channel shifts the bowl toward positive biases and the other toward negative biases. It is possible, in this case, that the bowl of the composite histogram has its minimum near  $V = 0$  V, but with asymmetric behavior on either side. Figures 7(c) and (d) show examples of this effect; the results are qualitatively similar to the experimental histogram in Figure 1(b).

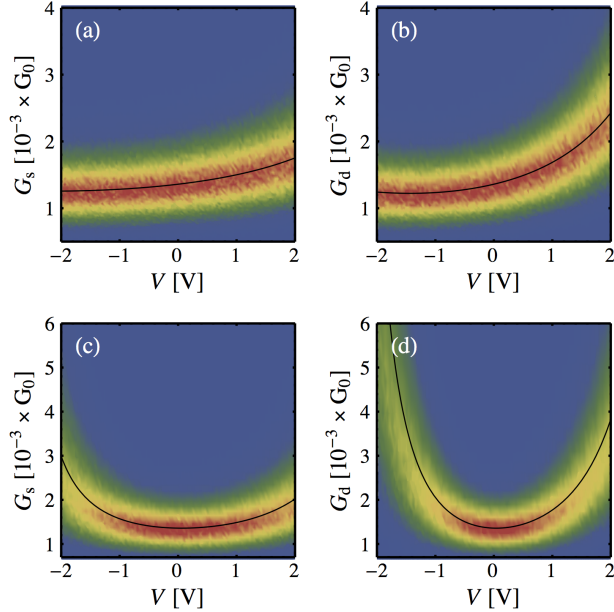


Figure 7: Simulated conductance histograms for two independent channels with  $\varepsilon_1 = -3.5 \pm 0.3$  eV,  $\Gamma_1 = 0.08 \pm 0.015$  eV,  $\varepsilon_2 = -3.8 \pm 0.3$  eV, and  $\Gamma_2 = 0.11 \pm 0.015$  eV. The left and right columns show static and differential conductance, respectively. (a) and (b)  $a_1 = 0.2$  and  $a_2 = 0.1$ .  $a_1$  and  $a_2$  have the same sign, and the minimum of the bowl is further shifted from  $V = 0$  V. (c) and (d)  $a_1 = -0.8$  and  $a_2 = 0.5$ . Because  $a_1$  and  $a_2$  have opposite signs, each channel contributes an symmetric bowl-shaped component to the total histogram; these minima are shifted in opposite directions. For some cases, such as that pictured here, the combined histogram through *both* channels can have its minimum near  $V = 0$  V but asymmetric behavior on either side of the minimum.

## 345 4 Conclusions

In this work we investigated the information content of voltage-dependent conductance histograms by developing and applying a framework for simulating such histograms. At the highest level, these histograms encode the shape of the transmission function near the Fermi

349 energy, giving rise to characteristic shapes. For non-resonant tunneling through a single  
350 channel (which is common for electrode-molecule-electrode junctions),  $T(E_F)$  is the tail of  
351 a Lorentzian, ultimately producing bowl-shaped histograms. The histogram is symmetric  
352 about its minimum and, in the absence of a voltage drop through the molecule, the mini-  
353 mum occurs at  $V = 0$  V. A voltage drop through the molecule (*i.e.*, when any of the model  
354 parameters depend on the bias) shifts the bowl’s minimum to non-zero biases. However,  
355 such a bowl remains symmetric about its minimum.

356 In the process of trying to qualitatively reproduce the experimental conductance his-  
357 tograms reported in Ref. 43, we also investigated the signatures of asymmetric channel-  
358 electrode couplings and of multi-channel effects in the histograms. First, the degree of  
359 asymmetric coupling is encoded in the skewness of the one-dimensional histogram peak for  
360 a particular bias. Such a one-dimensional conductance histogram is positively skewed (due  
361 of the shape of the transmission function for non-resonant tunneling<sup>53</sup>); asymmetric cou-  
362 pling makes the peak less skewed. Second, multi-channel effects can lead to a bowl-shaped  
363 histogram that is asymmetric about its minimum. In some cases, the combination of both  
364 channels produces a bowl with its minimum near  $V = 0$  V.

365 Taken collectively, our results show that voltage-dependent conductance histograms con-  
366 tain a wealth of information. Much of this data can be read from the shape of the histogram  
367 peak; in all cases here, the “average” conductance profile matched the histogram shape. We  
368 also did not find any qualitative differences between the static and differential conductance  
369 observables. In the end, our open source MolStat software<sup>60</sup> is designed to be extensible,  
370 facilitating the incorporation of additional model systems. It would be interesting, in future  
371 work, to identify any signatures of vibrational or inelastic effects on conductance histograms,  
372 and to further develop tools for extracting all of this information from the histograms.

373 **Acknowledgement**

374 We thank Nongjian Tao and his group for helpful conversations and for sharing the exper-

<sup>375</sup> imental data in Figure 1 with us. G. Z. performed this research as part of a Math-Science  
<sup>376</sup> Senior Thesis at the Oak Ridge High School. M. G. R. was supported by a Eugene P. Wigner  
<sup>377</sup> Fellowship while at the Oak Ridge National Laboratory, which is managed by UT-Battelle,  
<sup>378</sup> LLC, for the U.S. Department of Energy under contract DE-AC05-00OR22725. M. A. R.  
<sup>379</sup> and M. G. R. (while at Northwestern) were supported by the U.S. Air Force Office of Scien-  
<sup>380</sup> tific Research Multidisciplinary University Research Initiative (FA9550-14-1-003). M. A. R.  
<sup>381</sup> also thanks the Chemistry Division of the U.S. National Science Foundation for support  
<sup>382</sup> (CHE-1058896). The figures were prepared with the SciDraw package.<sup>61</sup>

## <sup>383</sup> Supporting Information Available

<sup>384</sup> The MolStat<sup>60</sup> input files used to generate the histograms analyzed in Figures 3, 4, 5, 6, and  
<sup>385</sup> 7 are presented in the Supporting Information. This material is available free of charge via  
<sup>386</sup> the Internet at <http://pubs.acs.org/>.

## <sup>387</sup> References

- <sup>388</sup> (1) Nitzan, A.; Ratner, M. A. Electron Transport in Molecular Wire Junctions. *Science*  
<sup>389</sup> **2003**, *300*, 1384–1389.
- <sup>390</sup> (2) Cuevas, J. C.; Scheer, E. *Molecular Electronics*; World Scientific (Hackensack, NJ,  
<sup>391</sup> USA), 2010.
- <sup>392</sup> (3) Karthäuser, S. Control of Molecule-Based Transport for Future Molecular Devices. *J.*  
<sup>393</sup> *Phys.: Condens. Matter* **2011**, *23*, 013001.
- <sup>394</sup> (4) Ratner, M. A Brief History of Molecular Electronics. *Nature Nanotech.* **2013**, *8*, 378–  
<sup>395</sup> 381.
- <sup>396</sup> (5) Imry, Y.; Landauer, R. Conductance Viewed as Transmission. *Rev. Mod. Phys.* **1999**,  
<sup>397</sup> *71*, S306–S312.

- 398 (6) Paulsson, M.; Brandbyge, M. Transmission Eigenchannels from Nonequilibrium Green's  
399 Functions. *Phys. Rev. B* **2007**, *76*, 115117.
- 400 (7) Kiguchi, M.; Tal, O.; Wohlthat, S.; Pauly, F.; Krieger, M.; Djukic, D.; Cuevas, J.;  
401 van Ruitenbeek, J. Highly Conductive Molecular Junctions Based on Direct Binding of  
402 Benzene to Platinum Electrodes. *Phys. Rev. Lett.* **2008**, *101*, 046801.
- 403 (8) Bergfield, J. P.; Barr, J. D.; Stafford, C. A. The Number of Transmission Channels  
404 Through a Single-Molecule Junction. *ACS Nano* **2011**, *5*, 2707–2714.
- 405 (9) Bergfield, J. P.; Barr, J. D.; Stafford, C. A. Transmission Eigenvalue Distributions in  
406 Highly Conductive Molecular Junctions. *Beilstein J. Nanotechnol.* **2012**, *3*, 40–51.
- 407 (10) Yaliraki, S. N.; Ratner, M. A. Molecule-Interface Coupling Effects on Electronic Trans-  
408 port in Molecular Wires. *J. Chem. Phys.* **1998**, *109*, 5036–5043.
- 409 (11) Xu, B.; Tao, N. J. Measurement of Single-Molecule Resistance by Repeated Formation  
410 of Molecular Junctions. *Science* **2003**, *301*, 1221–1223.
- 411 (12) Li, X.; He, J.; Hihath, J.; Xu, B.; Lindsay, S. M.; Tao, N. Conductance of Single  
412 Alkanedithiols: Conduction Mechanism and Effect of MoleculeElectrode Contacts. *J.  
413 Am. Chem. Soc.* **2006**, *128*, 2135–2141.
- 414 (13) Venkataraman, L.; Klare, J. E.; Tam, I. W.; Nuckolls, C.; Hybertsen, M. S.; Steiger-  
415 wald, M. L. Single-Molecule Circuits with Well-Defined Molecular Conductance. *Nano  
416 Lett.* **2006**, *6*, 458–462.
- 417 (14) Chen, F.; Hihath, J.; Huang, Z.; Li, X.; Tao, N. J. Measurement of Single-Molecule  
418 Conductance. *Annu. Rev. Phys. Chem.* **2007**, *58*, 535–564.
- 419 (15) Li, C.; Pobelov, I.; Wandlowski, T.; Bagrets, A.; Arnold, A.; Evers, F. Charge Trans-  
420 port in Single Au — Alkanedithiol — Au Junctions: Coordination Geometries and  
421 Conformational Degrees of Freedom. *J. Am. Chem. Soc.* **2008**, *130*, 318–326.

- 422 (16) Andrews, D. Q.; Van Duyne, R. P.; Ratner, M. A. Stochastic Modulation in Molecular  
423 Electronic Transport Junctions: Molecular Dynamics Coupled with Charge Transport  
424 Calculations. *Nano Lett.* **2008**, *8*, 1120–1126.
- 425 (17) Hybertsen, M. S.; Venkataraman, L.; Klare, J. E.; Whalley, A. C.; Steigerwald, M. L.;  
426 Nuckolls, C. Amine-Linked Single-Molecule Circuits: Systematic Trends Across Molec-  
427 ular Families. *J. Phys.: Condens. Matter* **2008**, *20*, 374115.
- 428 (18) Haiss, W.; Martín, S.; Leary, E.; van Zalinge, H.; Higgins, S. J.; Bouffier, L.;  
429 Nichols, R. J. Impact of Junction Formation Method and Surface Roughness on Single  
430 Molecule Conductance. *J. Phys. Chem. C* **2009**, *113*, 5823–5833.
- 431 (19) Paulsson, M.; Krag, C.; Frederiksen, T.; Brandbyge, M. Conductance of Alkanedithiol  
432 Single-Molecule Junctions: A Molecular Dynamics Study. *Nano Lett.* **2009**, *9*, 117–121.
- 433 (20) Hong, W.; Manrique, D. Z.; Moreno-García, P.; Gulcur, M.; Mishchenko, A.; Lam-  
434 bert, C. J.; Bryce, M. R.; Wandlowski, T. Single Molecular Conductance of Tolanes:  
435 Experimental and Theoretical Study on the Junction Evolution Dependent on the An-  
436 choring Group. *J. Am. Chem. Soc.* **2012**, *134*, 2292–2304.
- 437 (21) Paz, S. A.; Michoff, M. E. Z.; Negre, C. F. A.; Olmos-Asar, J. A.; Mariscal, M. M.;  
438 Sánchez, C. G.; Leiva, E. P. M. Anchoring Sites to the STM Tip Can Explain Multiple  
439 Peaks in Single Molecule Conductance Histograms. *Phys. Chem. Chem. Phys.* **2013**,  
440 *15*, 1526–1531.
- 441 (22) Konishi, T.; Kiguchi, M.; Takase, M.; Nagasawa, F.; Nabika, H.; Ikeda, K.; Uosaki, K.;  
442 Ueno, K.; Misawa, H.; Murakoshi, K. Single Molecule Dynamics at a Mechanically  
443 Controllable Break Junction in Solution at Room Temperature. *J. Am. Chem. Soc.*  
444 **2013**, *135*, 1009–1014.
- 445 (23) French, W. R.; Iacobella, C. R.; Rungger, I.; Souza, A. M.; Sanvito, S.; Cummings, P. T.

- 446 Structural Origins of Conductance Fluctuations in Gold–Thiolate Molecular Transport  
447 Junctions. *J. Phys. Chem. Lett.* **2013**, *4*, 887–891.
- 448 (24) Hihath, J.; Tao, N. The Role of Molecule–Electrode Contact in Single-Molecule Elec-  
449 tronics. *Semicond. Sci. Technol.* **2014**, *29*, 054007.
- 450 (25) Ding, W.; Negre, C. F. A.; Vogt, L.; Batista, V. S. High-Conductance Conformers  
451 in Histograms of Single-Molecule Current–Voltage Characteristics. *J. Phys. Chem. C*  
452 **2014**, *118*, 8316–8321.
- 453 (26) Afsari, S.; Li, Z.; Borguet, E. Orientation-Controlled Single-Molecule Junctions. *Angew.*  
454 *Chem. Int. Ed.* **2014**, DOI:10.1002/anie.201402343.
- 455 (27) Bilić, A.; Reimers, J. R.; Hush, N. S. The Structure, Energetics, and Nature of the  
456 Chemical Bonding of Phenylthiol Adsorbed on the Au(111) Surface: Implications for  
457 Density-Functional Calculations of Molecular-Electronic Conduction. *J. Chem. Phys.*  
458 **2005**, *122*, 094708.
- 459 (28) He, J.; Sankey, O.; Lee, M.; Tao, N.; Li, X.; Lindsay, S. Measuring Single Molecule  
460 Conductance with Break Junctions. *Faraday Discuss.* **2006**, *131*, 145–154.
- 461 (29) Meisner, J. S.; Ahn, S.; Aradhya, S. V.; Krikorian, M.; Parameswaran, R.; Steiger-  
462 wald, M.; Venkataraman, L.; Nuckolls, C. Importance of Direct Metal-π Coupling in  
463 Electronic Transport Through Conjugated Single-Molecule Junctions. *J. Am. Chem.*  
464 *Soc.* **2012**, *134*, 20440–20445.
- 465 (30) Kim, T.; Darancet, P.; Widawsky, J. R.; Kotiuga, M.; Quek, S. Y.; Neaton, J. B.;  
466 Venkataraman, L. Determination of Energy Level Alignment and Coupling Strength in  
467 4,4-Bipyridine Single-Molecule Junctions. *Nano Lett.* **2014**, *14*, 794–798.
- 468 (31) Mujica, V.; Kemp, M.; Roitberg, A.; Ratner, M. A. Current-Voltage Characteristics of

- 469 Molecular Wires: Eigenvalue Staircase, Coulomb Blockade, and Rectification. *J. Chem.*  
470 *Phys.* **1996**, *104*, 7296–7305.
- 471 (32) Xiao, X.; Xu, B.; Tao, N. J. Measurement of Single Molecule Conductance: Ben-  
472 zenedithiol and Benzenedimethanethiol. *Nano Lett.* **2004**, *4*, 267–271.
- 473 (33) Lörtscher, E.; Weber, H. B.; Riel, H. Statistical Approach to Investigating Transport  
474 through Single Molecules. *Phys. Rev. Lett.* **2007**, *98*, 176807.
- 475 (34) Haiss, W.; Nichols, R. J.; van Zalinge, H.; Higgins, S. J.; Bethell, D.; Schiffrin, D. J.  
476 Measurement of Single Molecule Conductivity using the Spontaneous Formation of  
477 Molecular Wires. *Phys. Chem. Chem. Phys.* **2004**, *6*, 4330–4337.
- 478 (35) Mayor, M.; Weber, H. B. Statistical Analysis of Single-Molecule Junctions. *Angew.*  
479 *Chem. Int. Ed.* **2004**, *43*, 2882–2884.
- 480 (36) Engelkes, V. B.; Beebe, J. M.; Frisbie, C. D. Analysis of the Causes of Variance in  
481 Resistance Measurements on MetalMoleculeMetal Junctions Formed by Conducting-  
482 Probe Atomic Force Microscopy. *J. Phys. Chem. B* **2005**, *109*, 16801–16810.
- 483 (37) Ulrich, J.; Esrail, D.; Pontius, W.; Venkataraman, L.; Millar, D.; Doerrer, L. H. Vari-  
484 ability of Conductance in Molecular Junctions. *J. Phys. Chem. B* **2006**, *110*, 2462–2466.
- 485 (38) Venkataraman, L.; Klare, J. E.; Nuckolls, C.; Hybertsen, M. S.; Steigerwald, M. L. De-  
486 pendence of Single-Molecule Junction Conductance on Molecular Conformation. *Nature*  
487 **2006**, *442*, 904–907.
- 488 (39) Jang, S.-Y.; Reddy, P.; Majumdar, A.; Segalman, R. A. Interpretation of Stochastic  
489 Events in Single Molecule Conductance Measurements. *Nano Lett.* **2006**, *6*, 2362–2367.
- 490 (40) González, M. T.; Wu, S.; Huber, R.; van der Molen, S. J.; Schönenberger, C.;  
491 Calame, M. Electrical Conductance of Molecular Junctions by a Robust Statistical  
492 Analysis. *Nano Lett.* **2006**, *6*, 2238–2242.

- 493 (41) Nichols, R. J.; Haiss, W.; Higgins, S. J.; Leary, E.; Martín, S.; Bethell, D. The Exper-  
494       imental Determination of the Conductance of Single Molecules. *Phys. Chem. Chem.*  
495       *Phys.* **2010**, *12*, 2801–2815.
- 496 (42) Leary, E.; González, M. T.; van der Pol, C.; Bryce, M. R.; Filippone, S.; Martín, N.;  
497       Rubio-Bollinger, G.; Agraït, N. Unambiguous One-Molecule Conductance Measure-  
498       ments under Ambient Conditions. *Nano Lett.* **2011**, *11*, 2236–2241.
- 499 (43) Guo, S.; Hihath, J.; Díez-Pérez, I.; Tao, N. Measurement and Statistical Analysis of  
500       Single-Molecule Current–Voltage Characteristics, Transition Voltage Spectroscopy, and  
501       Tunneling Barrier Height. *J. Am. Chem. Soc.* **2011**, *133*, 19189–19197.
- 502 (44) Natelson, D. Mechanical Break Junctions: Enormous Information in a Nanoscale Pack-  
503       age. *ACS Nano* **2012**, *6*, 2871–2876.
- 504 (45) Makk, P.; Tomaszewski, D.; Martinek, J.; Balogh, Z.; Csonka, S.; Wawrzyniak, M.;  
505       Frei, M.; Venkataraman, L.; Halbritter, A. Correlation Analysis of Atomic and Single-  
506       Molecule Junction Conductance. *ACS Nano* **2012**, *6*, 3411–3423.
- 507 (46) Frisenda, R.; Perrin, M. L.; Valkenier, H.; Hummelen, J. C.; van der Zant, H. S. J.  
508       Statistical Analysis of Single-Molecule Breaking Traces. *phys. status solidi (b)* **2013**,  
509       *250*, 2431–2436.
- 510 (47) Krans, J. M.; van Ruitenbeek, J. M.; Fisun, V. V.; Yanson, I. K.; de Jongh, L. J. The  
511       Signature of Conductance Quantization in Metallic Point Contacts. *Nature* **1995**, *375*,  
512       767–769.
- 513 (48) Bâldea, I. Interpretation of Stochastic Events in Single-Molecule Measurements of Con-  
514       ductance and Transition Voltage Spectroscopy. *J. Am. Chem. Soc.* **2012**, *134*, 7958–  
515       7962.

- 516 (49) Hines, T.; Díez-Pérez, I.; Hihath, J.; Liu, H.; Wang, Z.-S.; Zhao, J.; Zhou, G.;  
517 Müllen, K.; Tao, N. Transition from Tunneling to Hopping in Single Molecular Junc-  
518 tions by Measuring Length and Temperature Dependence. *J. Am. Chem. Soc.* **2010**,  
519 *132*, 11658–11664.
- 520 (50) Nakashima, S.; Takahashi, Y.; Kiguchi, M. Effect of the Environment on the Elec-  
521 trical Conductance of the Single Benzene-1,4-Diamine Molecule Junction. *Beilstein J.*  
522 *Nanotechnol.* **2011**, *2*, 755–759.
- 523 (51) Williams, P. D.; Reuter, M. G. Level Alignments and Coupling Strengths in Conduc-  
524 tance Histograms: The Information Content of a Single Channel Peak. *J. Phys. Chem.*  
525 *C* **2013**, *117*, 5937–5942.
- 526 (52) Ghahramani, S. *Fundamentals of Probability*, 2nd ed.; Prentice-Hall (Upper Saddle  
527 River, NJ, USA), 2000.
- 528 (53) Reuter, M. G.; Hersam, M. C.; Seideman, T.; Ratner, M. A. Signatures of Cooperative  
529 Effects and Transport Mechanisms in Conductance Histograms. *Nano Lett.* **2012**, *12*,  
530 2243–2248.
- 531 (54) Halbritter, A.; Makk, P.; Mackowiak, S.; Csonka, S.; Wawrzyniak, M.; Martinek, J.  
532 Regular Atomic Narrowing of Ni, Fe, and V Nanowires Resolved by Two-Dimensional  
533 Correlation Analysis. *Phys. Rev. Lett.* **2010**, *105*, 266805.
- 534 (55) Fock, J.; Sørensen, J. K.; Lörtscher, E.; Vosch, T.; Martin, C. A.; Riel, H.; Kilså, K.;  
535 Bjørnholm, T.; van der Zant, H. A Statistical Approach to Inelastic Electron Tunneling  
536 Spectroscopy on Fullerene-Terminated Molecules. *Phys. Chem. Chem. Phys.* **2011**, *13*,  
537 14325–14332.
- 538 (56) Hamill, J. M.; Wang, K.; Xu, B. Force and Conductance Molecular Break Junctions  
539 with Time Series Crosscorrelation. *Nanoscale* **2014**, *6*, 5657–5661.

- 540 (57) Büttiker, M.; Imry, Y.; Landauer, R.; Pinhas, S. Generalized Many-Channel Conduc-  
541 tance Formula with Application to Small Rings. *Phys. Rev. B* **1985**, *31*, 6207–6215.
- 542 (58) Economou, E. N. *Green's Functions in Quantum Physics*, 3rd ed.; Springer-Verlag (Hei-  
543 delberg, Germany), 2006.
- 544 (59) Galassi, M.; Davies, J.; Theiler, J.; Gough, B.; Jungman, G.; Alken, P.; Booth, M.;  
545 Rossi, F. *GNU Scientific Library Reference Manual*, 3rd ed.; Network Theory Ltd.,  
546 2009.
- 547 (60) <https://bitbucket.org/mgreuter/molstat>.
- 548 (61) Caprio, M. A. LevelScheme: A Level Scheme Drawing and Scientific Figure Preparation  
549 System for Mathematica. *Comput. Phys. Commun.* **2005**, *171*, 107–118.

550 Graphical TOC Entry

551

